Stem Cell Reports
Article

OPEN ACCESS

Abnormal Neural Progenitor Cells Differentiated from Induced Pluripotent Stem Cells Partially Mimicked Development of *TSC2* Neurological Abnormalities

Yaqin Li,[1,2,4] Jiqing Cao,[1,3,4] Menglong Chen,[1,4] Jing Li,[1] Yiming Sun,[1] Yu Zhang,[1] Yuling Zhu,[1] Liang Wang,[1] and Cheng Zhang[1,*]

[1]Department of Neurology, First Affiliated Hospital of Sun Yat-sen University, Guangzhou, Guangdong 510080, P.R. China
[2]Department of Neurology, Seventh Affiliated Hospital of Sun Yat-sen University, Shenzhen, Guangdong 518017, P.R. China
[3]Department of Neurology, The Central Hospital of Wuhan, Tongji Medical College, Huazhong University of Science and Technology, Wuhan 430014, P.R. China
[4]Co-first author
*Correspondence: zhangch6@mail.sysu.edu.cn
http://dx.doi.org/10.1016/j.stemcr.2017.02.020

SUMMARY

Tuberous sclerosis complex (TSC) is a disease featuring devastating and therapeutically challenging neurological abnormalities. However, there is a lack of specific neural progenitor cell models for TSC. Here, the pathology of TSC was studied using primitive neural stem cells (pNSCs) from a patient presenting a c.1444-2A>C mutation in *TSC2*. We found that *TSC2* pNSCs had higher proliferative activity and increased PAX6 expression compared with those of control pNSCs. Neurons differentiated from *TSC2* pNSCs showed enlargement of the soma, perturbed neurite outgrowth, and abnormal connections among cells. *TSC2* astrocytes had increased saturation density and higher proliferative activity. Moreover, the activity of the mTOR pathway was enhanced in pNSCs and induced in neurons and astrocytes. Thus, our results suggested that *TSC2* heterozygosity caused neurological malformations in pNSCs, indicating that its heterozygosity might be sufficient for the development of neurological abnormalities in patients.

INTRODUCTION

Tuberous sclerosis complex (TSC) is an autosomal-dominant disorder characterized by hamartomas in multiple organs with an incidence of approximately 1 in 6,000 at birth (Orlova and Crino, 2010). It is caused by mutations in either *TSC1* or *TSC2*, which encode the proteins hamartin and tuberin, respectively (Kandt et al., 1992; van Slegtenhorst et al., 1997). Hamartin and tuberin bind to each other to form a heterodimer that can inhibit the activation of mammalian target of rapamycin (mTOR), which regulates protein synthesis, cell growth, and proliferation (Long et al., 2005). Despite reports implying that a second-hit mutation is sufficient for the development of TSC, loss of heterozygosity is difficult to demonstrate in brain lesions and was observed in only 4% of the cortical tubers and subependymal nodules assayed in a previous study (Henske et al., 1996). Further investigation is needed to confirm whether *TSC1* or *TSC2* heterozygosity is sufficient for the development of neurological abnormalities.

Patient-specific induced pluripotent stem cells (iPSCs), which can model the pathology of a specific disease, represent a promising resource for studying disease mechanisms, screening for novel drug compounds, and developing new therapies (Ebert et al., 2009). The generation of expandable primitive neural stem cells (pNSCs) from iPSCs and their further differentiation into neuron and astrocyte lineages (Yan et al., 2013) enables modeling of human neurological diseases at the cellular level.

During the last decade, it was demonstrated that a *TSC1* defect in embryonic neural progenitor cells caused CNS malformations similar to those observed in patients with TSC by using $TSC1^{Emx1-Cre}$ conditional knockout animals (Carson et al., 2012). Therefore, the isolation and molecular characterization of TSC-specific pNSCs would provide a powerful model for studying the abnormal neural development that occurs in TSC and the potential underlying mechanisms.

mTOR is a serine/threonine protein kinase that forms two distinct multiprotein complexes, mTORC1 and mTORC2, and stimulates protein translation by activating downstream targets, including eIF4E/4E-binding protein and p70S6 kinase/ribosomal S6 protein. mTOR regulates neuronal proliferation, survival, growth, and function, which are critical for development, and deregulation of mTOR at any stage of development can have deleterious consequences. Cell populations expressing hyperactive mTOR show many structural abnormalities that support recurrent circuit formation, including somatic and dendritic hypertrophy, aberrant basal dendrites, and axon-tract enlargement. At the functional level, mTOR hyperactivation is commonly but not always associated with enhanced synaptic transmission and plasticity (Lasarge and Danzer, 2014). The mTORC1 inhibitor everolimus (an analog of rapamycin) is now recommended for the

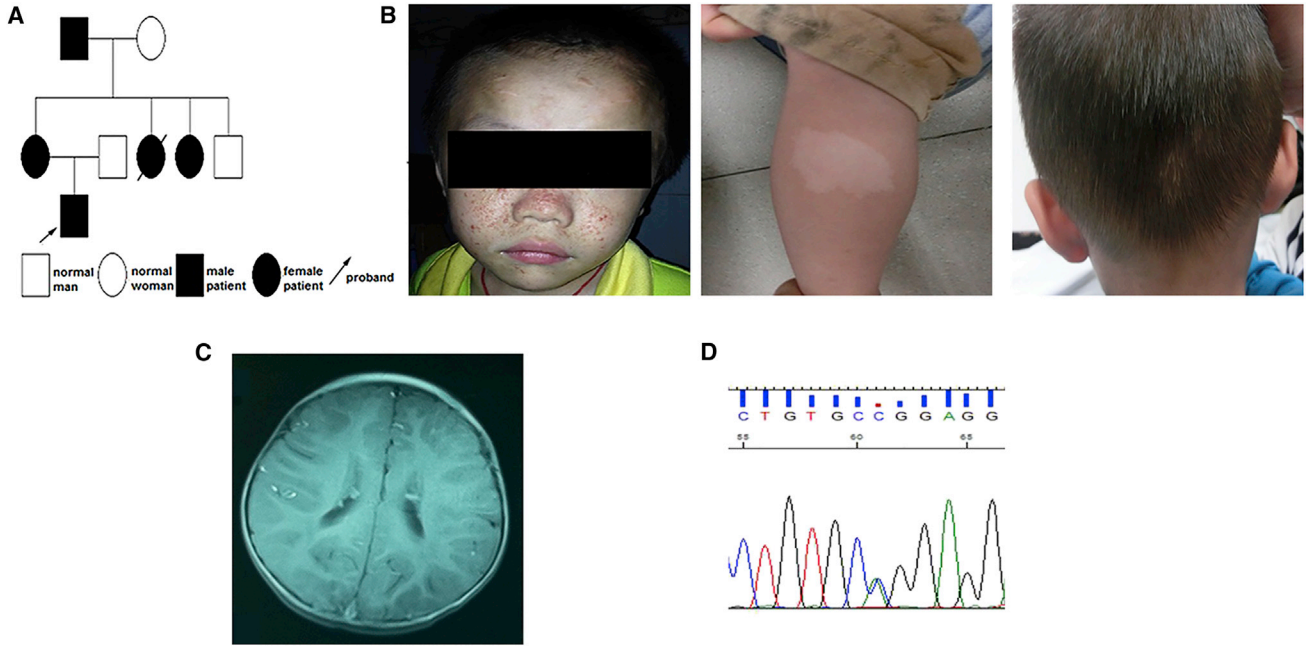

Figure 1. Clinical Characteristics of the Patient with Tuberous Sclerosis Complex

(A) Pedigree of the patient's family.

(B) Physical examination showed facial angiofibroma, white macules, and an occipital patch of poliosis.

(C) Brain MRI showed subependymal nodules in the lateral ventricles.

(D) Sequencing of *TSC2* from the TSC patient revealed a c.1444-2A>C mutation.

treatment of subependymal giant cell astrocytomas and renal angiomyolipoma in tuberous sclerosis. However, the molecular mechanism underlying the development and pathologies of TSC is not yet fully understood.

Therefore, in this study, we assessed the potential of iPSCs obtained from the peripheral blood of a proband of a TSC pedigree who presented with neurological abnormalities to develop a cellular model of *TSC2* deficiency. pNSCs, neurons, and astrocytes were differentiated from the iPSCs to study the cellular pathology and underlying mechanisms of TSC.

RESULTS

Clinical Characteristics of the Family

The patient was a 2-year-old boy (Figure 1A) who was diagnosed with TSC when he was examined for epilepsy. He also had minor intellectual disability, facial angiofibroma, white macules, and, interestingly, an occipital patch of poliosis (Figure 1B). The cortical tubers and subependymal nodules were visible on a brain MRI scan (Figure 1C). Except for his younger aunt, who died of epilepsy, his mother, elder aunt, and grandfather presented nearly normal intelligence and no epilepsy, but presented with facial angiofibroma, white macules, ungual fibroma, or a shagreen patch on the skin. His grandfather also presented with a kidney angiomyolipoma. An MRI scan of the brain of his elder aunt also showed subependymal nodules. A c.1444-2A>C mutation in the *TSC2* gene (GenBank: NM_000548.4; Figure 1D), which is predicted to cause a splicing error (Kwiatkowski et al., 2015; Tyburczy et al., 2014), was detected in all family members by *TSC1*/*TSC2* gene mutation analysis.

Generation of iPSC Lines from the TSC Patient's Peripheral Blood Mononuclear Cells

The protocol used to obtain iPSCs from the patient's and unaffected control's peripheral blood mononuclear cells (PBMCs) is summarized in Figure 2A. Human embryonic stem cell-like colonies were picked on day 16 after transduction and passaged manually. The iPSC lines showed the typical morphology of human embryonic stem cells in feeder-free conditions (Figure 2B). These lines expressed pluripotency marker proteins including OCT4, SOX2, SSEA4, and TRA-1-81 (Figures 2C and S1A). During in vitro differentiation, the clones could produce three embryonic germ layers (i.e., the endoderm, mesoderm, and ectoderm) as revealed by the expression of AFP, SMA, and NESTIN, respectively (Figures 2D and S1B).

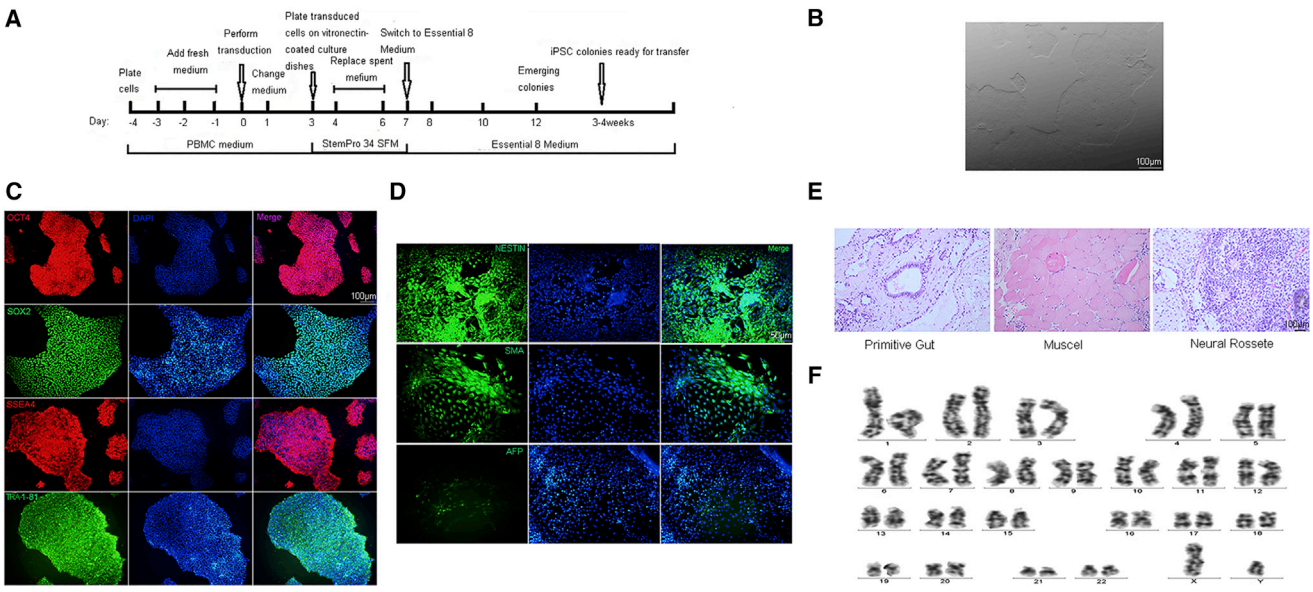

Figure 2. Generation and Identification of Induced Pluripotent Stem Cells from the TSC Patient

(A) Experimental scheme for the generation of iPSCs from peripheral blood mononuclear cells.

(B) Morphology of iPSC lines in feeder-free medium. Scale bar, 100 μm.

(C) Immunofluorescence for the pluripotency markers OCT4, SOX2, SSEA4, and TRA-1-81 in iPSC lines. Scale bar, 100 μm.

(D) Immunofluorescence for the endoderm (α-fetoprotein [AFP]), mesoderm (smooth muscle actin [SMA]), and ectoderm (NESTIN) markers in iPSC lines. Scale bar, 50 μm.

(E) Teratoma formation for the TSC-patient-derived iPSC line shows tissues from the three germ layers. Scale bar, 100 μm.

(F) Karyotype analysis of iPSC lines.

See also Figures S1–S3.

The in vivo differentiation ability of these derived iPSC lines was assessed by teratoma formation assay. Teratoma-containing cells derived from the three embryonic germ layers were observed in non-obese diabetic (NOD)/severe combined immunodeficiency (SCID) mice (Figures 2E and S1C). The TSC iPSCs maintained normal karyotypes (Figures 2F and S1D). *TSC1*/*TSC2* mutation analysis of the iPSCs derived from the TSC patient and an unaffected control showed that the TSC iPSCs had a c.1444-2A>C mutation in the *TSC2* gene, while unaffected iPSCs did not have any detectable mutation (Figure S2A). Moreover, pS6 expression was substantially higher in TSC iPSCs than in the unaffected controls (Figure S3). Three iPSC lines from the TSC patient (TSC) and three iPSC lines generated from two sex-matched unaffected controls (CTL) (one of the unaffected control iPSC lines was a kind gift from Prof. Sun of The Third Hospital of Guang Zhou Medical University) were selected for further experiments on neural differentiation.

Derivation of pNSCs from iPSCs

Previous studies suggested that TSC tubers may arise from *TSC1* or *TSC2* deficiency in neural progenitor cells. To investigate the effects of *TSC2* deficiency in neural progenitor cells, TSC pNSCs were generated from TSC iPSCs and compared with unaffected control pNSCs (Figure 3A). Cells from the second passage were dissociated and plated for neural stem cell (NSC) marker immunostaining. Most of the cells expressed NSC markers, including NESTIN, SOX1, and SOX2 (Figure 3B). These results were confirmed by flow cytometry. The vast majority of the cells expressed SOX1 and NESTIN (Figures 3C and 3D). In contrast with the control cells, TSC pNSCs highly expressed PAX6 (TSC versus unaffected control, 58.01% ± 6.97%; 12.96% ± 5.53%, p = 0.001) (Figures 3C and 3D). *TSC1*/*TSC2* mutation analysis of the pNSCs derived from the TSC patient and unaffected control showed that the TSC-patient-specific pNSCs had the same *TSC2* mutation as that found in the patient's blood (Figure S2A). In addition, variant transcripts amplified by primer sets targeting sequences around the *TSC2* c.1444_2A>C mutation were found in TSC pNSCs compared with control pNSCs (Figure S2B). cDNA sequence chromatograms obtained by Sanger sequencing of *TSC2* exon13F/intron14R showed an mRNA sequence that was lengthened by 122 bp owing to intron retention in the TSC pNSCs compared with that in control pNSCs (Figure S2C). This mutation is predicted to encode a truncated protein

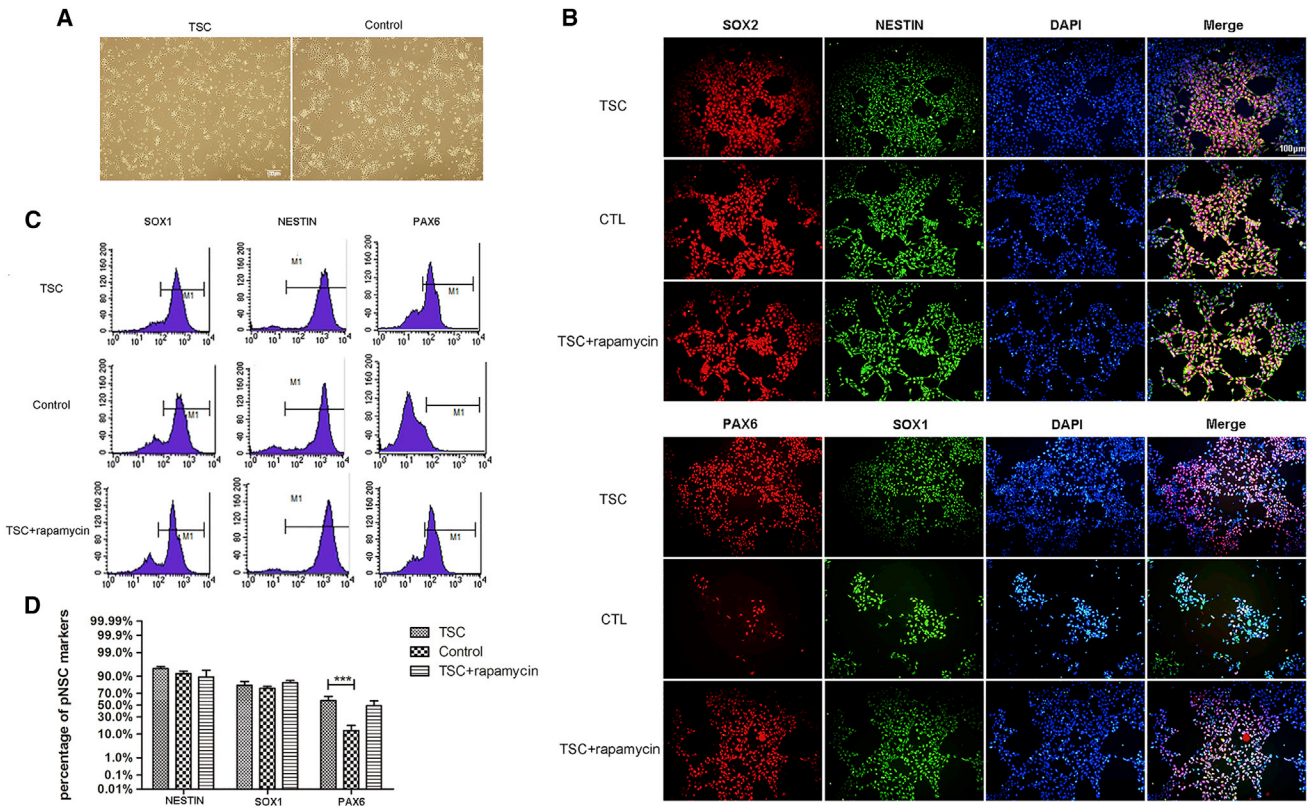

Figure 3. Derivation and Activation of Primitive Neural Stem Cells from Patient-Specific iPSCs

(A) Phase microphotographs of TSC and control pNSCs. Scale bar, 100 μm.

(B) Immunofluorescence of pNSCs differentiated from the TSC patient, normal controls, and rapamycin-treated iPSCs, showing the expression of the markers NESTIN, SOX1, PAX6, and SOX2. Scale bar, 100 μm.

(C and D) Flow cytometry analysis of pNSCs from the TSC patient, normal controls, and rapamycin-treated iPSCs using the neural stem cell markers NESTIN, SOX1, and PAX6 (n = 3 independent experiments, mean ± SEM; ***p < 0.005; Student's t test). Scale bar, 100 μm.

(55.4 kDa, http://web.expasy.org/compute_pi/), which should result in reduced levels of the mutant transcript because of a mechanism known as nonsense-mediated mRNA decay (Jeganathan et al., 2002). To test that prediction, TUBERIN expression was detected using antibodies against epitopes of TUBERIN-N and TUBERIN-C. Both TSC pNSCs and control pNSCs expressed normal TUBERIN protein, but its expression was higher in control pNSCs than in TSC pNSCs (Figure S2D). The 122-bp extension of the *TSC2* transcript owing to intron retention and the low expression level of TUBERIN protein in TSC pNSCs confirmed that the mutation in the *TSC2* gene directly causes TSC. Therefore, these cells can be used as a model to explore the pathogenesis of TSC.

High Proliferation and Activation of the mTOR Pathway in TSC pNSCs

As previously described, the growth characteristics of wild-type (WT), *TSC2* haploinsufficient, and *TSC2* knockout murine neuroepithelial progenitor cells were similar (Onda, 2002). However, another study demonstrated that *TSC2* haploinsufficient embryonic telencephalic NSCs had a higher rate of self-renewal than the WT and mutant cells did (Magri et al., 2011). Thus, to investigate the effects of *TSC2* deficiency in human pNSCs, CCK8 proliferation assay and 5-bromo-2-deoxyuridine (BrdU) staining were performed to measure their proliferation rate. Compared with CTL pNSCs, TSC pNSCs presented a higher growth rate (TSC versus control BrdU, 0.58 ± 0.02 versus 0.51 ± 0.02, p = 0.09). Moreover, rapamycin treatment decreased proliferation (TSC versus TSC + rapamcyin BrdU, 0.58 ± 0.02 versus 0.02 ± 0.10, p < 0.001; CTL versus CTL + rapamycin BrdU, 0.51 ± 0.02 versus 0.18 ± 0.02, p < 0.001), indicating that the increase in proliferation might be due to activation of the mTOR pathway (Figures 4A–4C and S4). Phosphorylated S6 (pS6) and AKT (pAKT) are established biomarkers for the activation of the mTORC1 and mTORC2 signaling pathways, respectively. Increased expression levels of both pS6 and pAKT were observed (TSC versus CTL pS6, 0.20 ± 0.01 versus 0.11 ± 0.01,

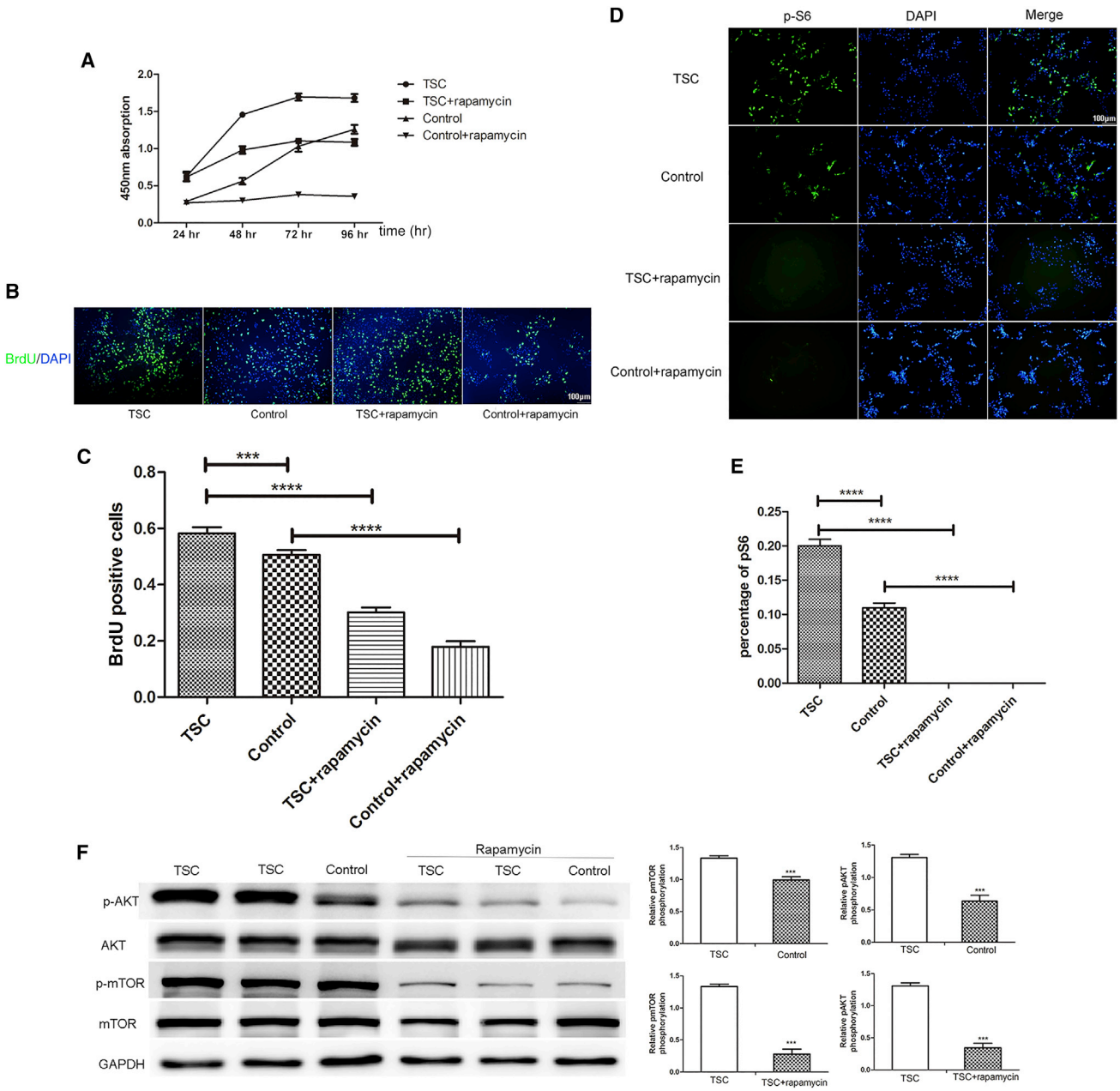

Figure 4. High Proliferation Rate and mTOR Pathway Activation in TSC Haploinsufficient pNSCs

(A) CCK8 detection in *TSC* haploinsufficient and normal control pNSCs treated with or without rapamycin for 24, 48, and 72 hr. The absorbance was detected at 24, 48, 72, and 96 hr (n = 3 independent experiments, mean ± SEM).

(B and C) BrdU staining (n = 3 independent experiments, mean ± SEM; ***p < 0.005, ****p < 0.001; Student's t test). Scale bar, 100 μm.

(D and E) Increased S6 phosphorylation in TSC pNSCs. (n = 3–4 independent experiments, mean ± SEM; ****p < 0.001; Student's t test). Scale bar, 100 μm.

(F) mTOR pathway activation in pNSCs as evaluated by western blot analysis. Expression levels were normalized to that of glyceraldehyde-3-phosphate (GAPDH) (n = 3 independent experiments, mean ± SEM; ***p < 0.005; Student's t test).

See also Figure S4.

p < 0.001), suggesting that both the mTORC1 and mTORC2 pathways were activated. Moreover, phosphorylated mTOR (p-mTOR) and phosphorylated AKT expression were increased as expected (Figures 4D–4F). There were no changes in AKT and mTOR expression. Rapamycin significantly decreased the expression of pS6, pAKT, and

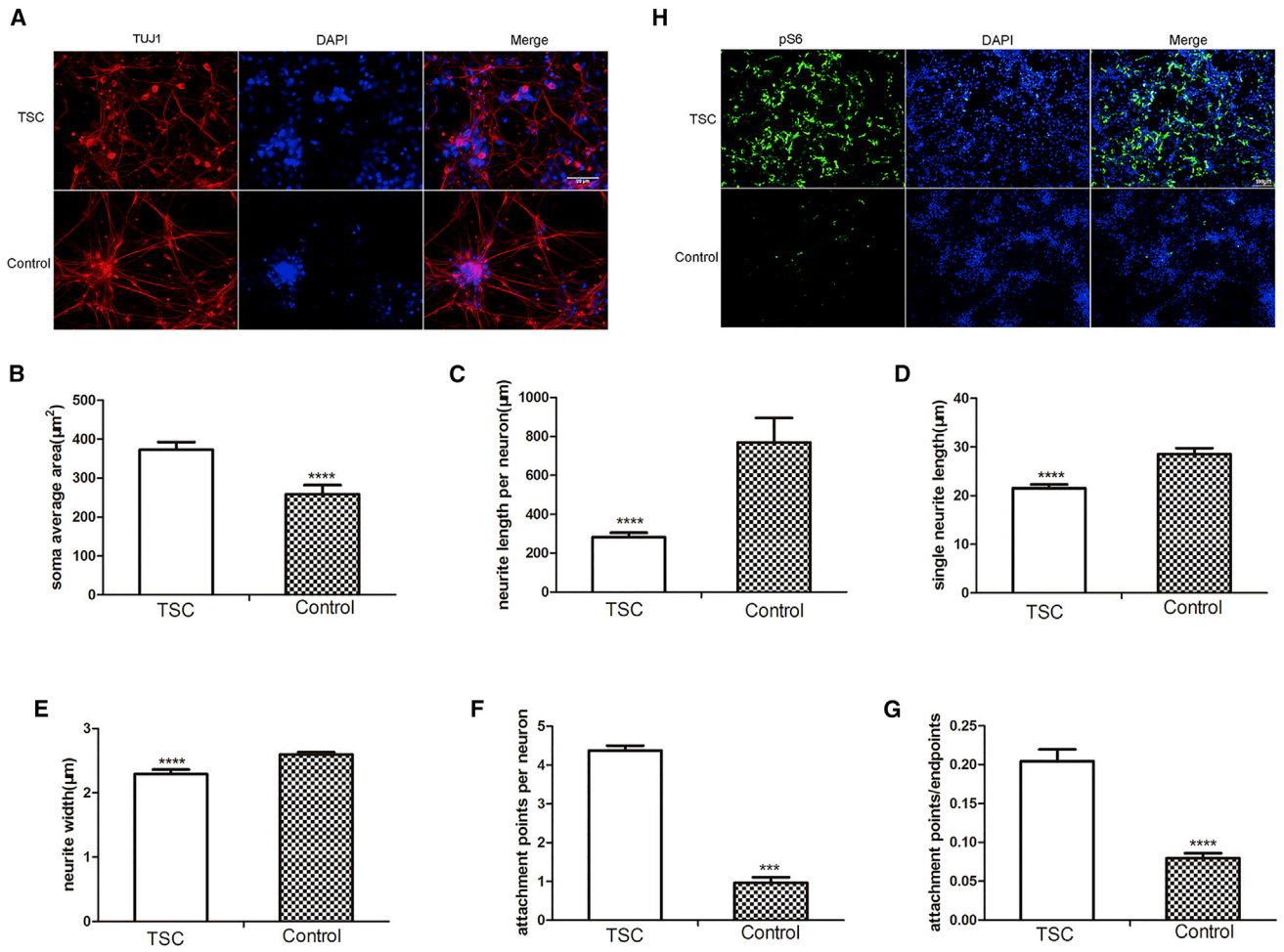

Figure 5. Differentiation of TSC pNSCs into Neurons

(A–G) Immunofluorescence images (A) of neurons differentiated from the patient with TSC and the unaffected controls showing the expression of β-III-TUBULIN and the morphology of the neurons differentiated from the patient with TSC and the unaffected controls as determined using NeurphologyJ (B–G; n = 3 independent experiments, mean ± SEM; ***p < 0.005, ****p < 0.001; Student's t test). Scale bar, 20 μm.

(H) Increased S6 phosphorylation in *TSC* neurons. Scale bar, 100 μm.

See also Figure S5.

p-mTOR, which is consistent with previous findings in TSC tubers.

Morphological Effects of TSC2 Haploinsufficiency

Previous studies demonstrated that the TSC mTOR pathway regulates the growth and synaptic functions of neurons in mice and rats, which may partially contribute to the pathogenesis of TSC (Tavazoie et al., 2005). To demonstrate the effect of *TSC2* deficiency in human neurons, pNSCs were induced to differentiate into neurons, as previously described (Yan et al., 2013). The vast majority of neurons expressed the neuronal markers TUJ1 and MAP2 but were devoid of glial fibrillary acidic protein (GFAP) expression (Figure S5). Moreover, atypical neuronal morphology was observed, and the soma size was higher in TSC neurons versus control neurons (372.92 ± 19.66 versus 259.04 ± 22.77 μm^2). The mean single neurite length and neurite length per neuron were significantly reduced in TSC neurons (21.53 ± 0.77 and 282.97 ± 22.42 μm, respectively) compared with those of control neurons (28.53 ± 1.21 and 769.49 ± 126.34 μm, respectively). Neurite width was also decreased in TSC neurons versus control neurons (2.29 ± 0.07 versus 2.60 ± 0.04 μm). The density of attachment points/endpoints increased (4.38 ± 0.13 versus 3.69 ± 0.14), which indicated more complex neurite branching (Figures 5A–5G). In addition, pS6 expression was substantially higher in TSC neurons (Figure 5H). As previously observed in mice and rats, *TSC2* haploinsufficiency in

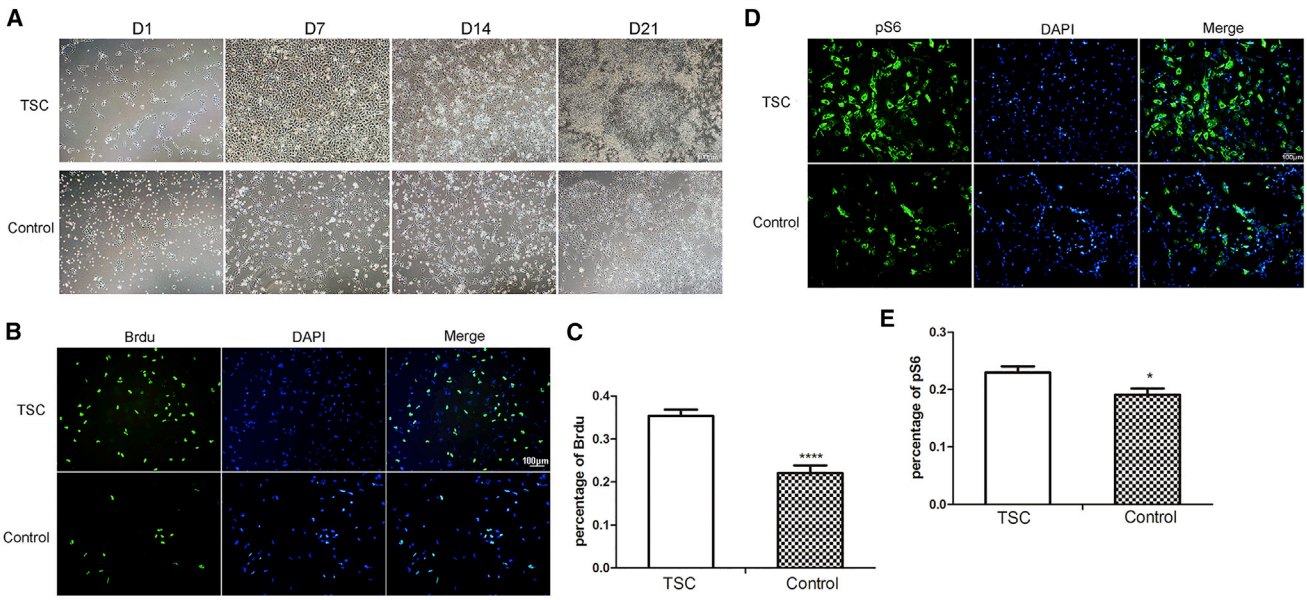

Figure 6. High Proliferation Rate and mTOR Pathway Activation in TSC Astrocytes

(A) Phase microphotographs of TSC and control astrocytes on days 1, 7, 14, and 21.

(B and C) BrdU staining of TSC and control astrocytes (n = 3 independent experiments, mean ± SEM; ****p < 0.001; Student's t test). Scale bar, 100 μm.

(D and E) Increased S6 phosphorylation in TSC astrocytes (n = 3 independent experiments, mean ± SEM; *p < 0.05; Student's t test). Scale bar, 100 μm.

human neurons was sufficient to trigger the enlargement of cell somas and dendritic spines and to increase the expression of pS6.

Proliferation of TSC Astrocytes Differentiated from pNSCs

Although no difference was detected in saturation density between *TSC2* haploinsufficient and WT astrocytes, both *TSC2* knockout fibroblasts and *TSC1* knockout astrocytes formed foci when grown to confluence and exhibited a higher saturation density than did the controls (Uhlmann et al., 2002). To determine whether *TSC2* heterozygosity presented the same growth advantage in human astrocytes, the *TSC2* pNSCs were induced to differentiate into astrocytes. Both differentiated astrocytes expressed GFAP (Figure S5). *TSC2* astrocytes were morphologically indistinguishable from control astrocytes. However, *TSC2* haploinsufficient astrocytes grew continuously after reaching confluency, while control astrocytes did not (Figure 6A). To examine cell proliferation during differentiation, BrdU staining was conducted at day 7 when the cells reached confluency. *TSC2* astrocytes presented a higher growth rate (TSC versus CTL, 0.35 ± 0.02 versus 0.22 ± 0.02, $p < 0.001$) and a higher level of pS6 (TSC versus CTL pS6, = 0.23 ± 0.01 versus 0.19 ± 0.01, $p = 0.015$) than did control astrocytes (Figures 6B and 6C).

DISCUSSION

TSC is an autosomal genetic disorder attributed to mutations in *TSC1* or *TSC2* with complex genotype-phenotype linkage, as in the pedigree observed in our study. TSC neurologic and psychiatric symptoms cause the most significant patient morbidity. Understanding the abnormal brain development that occurs in TSC and the underlying molecular mechanisms may yield therapies for intellectual disability , developmental delay, autism, and seizures in patients with TSC. Previous studies unraveled multi-lineage abnormalities in murine models of TSC. However, *TSC1* or *TSC2*$^{-}$ knockout mouse embryonic fibroblasts and heterozygous murine models failed to recapitulate tissue-specific features (Carson et al., 2012). Recently, CNS-specific TSC models that are able to reproduce specific features of the disease were generated (Magri et al., 2011). Therefore, in our study, we chose a proband from a TSC pedigree showing typical neurological abnormalities, *TSC2* heterozygosity, and a lack of response to pharmacotherapies including rapamycin.

During the reprogramming of fibroblasts (data not shown) and PBMCs into iPSCs, iPSCs that carried the TSC defect expanded robustly in culture and were similar to control iPSCs in terms of their morphology and pluripotency. Thus, the generation of iPSCs from a TSC patient's

cells provided access to pNSCs and neural cells to further explore the pathogenesis of the disease.

mTOR signaling functions in neural induction. Transcripts associated with mTOR (S6K1) were upregulated during neurogenesis (Fathi et al., 2011). In addition, the activation of mTOR upregulates the expression of PAX6 (Endo et al., 2009), which is important in various developmental processes in the CNS, including patterning of the neural tube, migration of neurons, and formation of neural circuits (Curto et al., 2014). According to our results, the activities of mTORC1 and mTORC2, as assessed by evaluating S6 and AKT phosphorylation, were upregulated in TSC pNSCs. The hyperactivation of the mTOR pathway enhanced the expression of neuroectodermal markers, especially PAX6. Therefore, the mTOR signaling pathway has important functions in the proliferation and differentiation of pNSCs. mTOR includes two structurally and functionally distinct complexes, mTOR complex 1 (mTORC1) and mTOR complex 2 (mTORC2) (Crino, 2011). Rapamycin can inhibit the activation of mTOR signaling through mTORC1, and it deregulated the proliferation of pNSCs in this study. Considering that *TSC2* deficiency caused cortical malformations early in pNSCs, while rapamycin decreased pNSC proliferation and the activation of the mTOR pathway, a preventive therapy for TSC would need to be administered to progenitor cells before the pNSC stage to reverse the neural and glial pathologies.

The TSC pathway regulates growth and synaptic functions in neurons. Perturbations in neuronal structure and function likely contribute to the pathogenesis and neurological symptoms of TSC in mice (Tavazoie et al., 2005). The functions of the *TSC1* and *TSC2* genes in mammalian neurons as well as the defects that arise from the hemizygosity of these genes are unknown. Notably, loss of *TSC1* or *TSC2* in mature post-mitotic hippocampal neurons in vitro causes enlarged somas, abnormal dendrites, and enhancement of glutamatergic neurotransmission. Loss of a single copy of *TSC1* was sufficient to perturb dendritic spine structure (Tavazoie et al., 2005). In this study, neurons differentiated from *TSC2* haploinsufficient pNSCs also presented with an enlarged soma, perturbed neurite outgrowth, complex neurite branching, and abnormal connections among neurons when compared with the WT neurons. Hyperactivation of the mTOR pathway supports recurrent circuit formation via stimulating neuronal changes, including somatic and dendritic hypertrophy, aberrant basal dendrites, and enlargement of axon tracts. In this study, mTOR was activated in neurons. Thus, *TSC2* haploinsufficiency was sufficient to induce changes in neuronal behavior resembling those that occur in TSC in vivo.

TSC haploinsufficient astrocytes presented a high proliferation rate and an increased saturation density when compared with WT astrocytes. Similarly, the conditional disruption of *TSC1* in astrocytes using a human GFAP-Cre system was shown to produce mice that presented with astrocytosis (Han and Sahin, 2011). Moreover, the increase in astrocyte proliferation may precede the neuronal abnormalities, resulting in hippocampal neuronal disorganization and seizures. Previous studies indicated that NESTIN-immunoreactive neural cells were less developed than mature astrocytes, raising the possibility that new neurons were generated from these NESTIN-positive progenitors, resulting in hippocampal neuronal disorganization. In addition, recent studies demonstrated that astrocytes could give rise to new neurons in the adult mammalian hippocampus (Seri et al., 2001). In our studies, we observed NESTIN and TUJ1 protein expression in differentiated astrocytes, while the differentiated neurons expressed TUJ1 and NESTIN (data not shown), but not GFAP. Thus, our results partially supported the hypothesis that hippocampal neuronal disorganization in TSC results from the aberrant differentiation of NESTIN-positive immature astrocytes into neurons. Further studies are warranted to confirm our results. In other studies, while both *TSC1* and *TSC2* heterozygous mice exhibited an increased number of astrocytes in vivo, there was no increase in the saturation density of *TSC2* haploinsufficient astrocytes compared with that of WT astrocytes in vitro. In addition, *TSC1* knockout astrocytes and *TSC1* knockout mouse embryonic fibroblasts presented a higher saturation density associated with decreased levels of $p27^{kip1}$ (Uhlmann et al., 2002). The authors suggested that the non-cell-autonomous growth advantage conferred by *TSC* heterozygosity may involve $p27^{kip1}$ expression. However, no gross or microscopic evidence of morphological brain abnormalities was detected in the *TSC1* or *TSC2* haploinsufficient mice, while our patient presented with tubers in the brain. However, we did not study $p27^{kip1}$ expression in our patient's astrocytes. Further experiments on the relationship between *TSC* heterozygosity and brain abnormalities, tuberin/hamartin signaling, and $p27^{kip1}$ expression are required.

The current study has some limitations. First, we did not investigate further the link between mTOR hyperactivation and synaptic transmission and plasticity, which might influence neuronal excitability and trigger epileptogenesis. However, a recent study on neurons derived from *TSC2*-deleted pluripotent stem cells demonstrated that heterozygous and homozygous loss of *TSC2* led to altered synaptogenesis and transmission and that pharmacological inhibition of mTORC1 could ameliorate synaptic dysfunction (Costa et al., 2016). Second, only the proband who was carrying *TSC2* gene mutation was compared with the normal control subject in our study. Identifying the possible role of *TSC* mutations in complex genetic and neural network processes pertaining to cell survival, structure, and function will provide a better understanding of the pathogenesis of

TSC-related neurological symptoms (Mayer et al., 2004; Talos et al., 2008). Although our results may partially confirm the pathophysiological mechanisms underlying the neurological manifestations in TSC, additional efforts must be undertaken to explore these mechanisms further.

In conclusion, abnormal pNSCs, neurons, and astrocytes differentiated from TSC iPSCs partially recapitulated the development of neurological abnormalities as observed in patients with mutations in *TSC2*, suggesting that *TSC1/2* haploinsufficiency might be sufficient to contribute to the neuropathology of TSC. Furthermore, these cells provide an unprecedented model for studying the abnormal neural development and the potential underlying mechanisms of TSC in vitro, screening novel drugs for personalized therapies, and potentially complementing/implementing mTOR-directed inhibitory approaches.

EXPERIMENTAL PROCEDURES

Ethics Statement

The study protocol was approved by the Ethics Committee at the First Affiliated Hospital of Sun Yat-sen University and written consent was obtained from the parents of the child from whom the peripheral blood was obtained.

Mutation Analysis

DNA from the patient's peripheral blood was extracted using a Blood Genomic DNA Extraction Kit (QIAGEN), and Phusion DNA polymerase was used for the amplification reaction, following the manufacturer's instructions. Amplification products were sequenced using an ABI PRISM 310 Genetic Analyzer (Applied Biosystems).

Derivation and Maintenance of the iPSC Line

PBMCs from the patient and from one sex-matched unaffected control donor were collected for iPSC induction. Cells were transduced with the integration-free CytoTune-iPS Sendai Reprogramming Kit (Life Technologies), which utilizes Sendai virus particles of the four Yamanaka factors. Transduced cells were plated on vitronectin-coated culture dishes and fed iPSC medium, which was replaced by StemPro 34 SFM (Life Technologies) from days 3 to 7. On day 7, the medium was replaced by Essential 8 medium (Life Technologies) until small colonies were formed. The growth of small colonies was maintained for another 3–4 weeks before each colony was picked for expansion into individual iPSC lines. The cell colonies were manually picked and mechanically dissociated for the first four passages. Next, iPSCs were passaged every 3–5 days using 0.5 mM EDTA (Life Technologies). Three colonies of the TSC proband, two colonies of the unaffected control, and one iPSC line from another unaffected control (gift from Prof. Sun) were picked for the following experiments.

Teratoma Formation

For teratoma formation, cells from one 60-mm dish were resuspended in a mixture of DMEM and Geltrex (ratio of 1:1) and injected intramuscularly into NOD/SCID mice. Teratoma formation occurred within 4–6 weeks and paraffin sections were stained with H&E. Animal experiments were performed in accordance with the Sun-Yet University Guidelines for Animal Care.

Karyotype Analysis

iPSCs were incubated in culture medium containing 0.25 μg/mL colcemid (Life Technologies) for 4 hr. Cells were then dissociated using 0.25% (w/v) trypsin, followed by a standard protocol for high-resolution G banding of chromosomes. Twenty chromosome spreads were examined.

Neural Stem Cell Induction of iPSCs and Expansion

iPSCs cultured in feeder-free conditions were passaged to six-well plates at a density of 2.5×10^4 cells/cm^2. Twenty-four hours after splitting, the culture medium was switched to Gibco PSC neural induction medium (Life Technologies) containing neurobasal medium and Gibco PSC neural induction supplement. After day 7 of induction, pNSCs were dissociated using Accutase (Life Technologies) and plated on Geltrex-coated dishes at a density of 1×10^5 cells per cm^2 in NSC expansion medium containing 50% (v/v) neural basal medium, 50% (v/v) advanced DMEM/F12, and 1× neural induction supplement. Before the fourth passage, cells were treated overnight with 5 μM Rho-associated protein kinase inhibitor, Y27632 (Sigma-Aldrich), which was added to the neural expansion medium at the time of NSC plating. Culture medium was replaced every other day, or every day depending on cell expansion.

Differentiation of TSC-Patient-Specific pNSCs into Neurons and Astrocytes

For neuronal differentiation, pNSCs induced from TSC-patient-specific iPSCs were passaged using Accutase and plated onto 10 μg/mL laminin-coated six-well chamber slides at a density of 4×10^4 cells/cm^2. Cells were cultured in neuronal differentiation medium containing 1× neurobasal medium, 2% (v/v) B-27 supplement, 2 mM (v/v) GlutaMAX supplement, 20 ng/mL brain-derived neurotrophic factor, 20 ng/mL glial cell-derived neurotrophic factor, 1× MEM non-essential amino acids solution (all from Life Technologies), and 200 μM L-ascorbic acid (Sigma-Aldrich) for 14 days. The culture medium was replaced every 2–3 days. For astrocyte differentiation, dissociated pNSCs were plated onto Geltrex-coated six-well chamber slides at a density of 2.5×10^4 cells/cm^2 in astrocyte differentiation medium (DMEM supplemented with N2 supplement and 1% [v/v] fetal bovine serum; Life Technologies) for 21 days. Confluent cultures were passaged at a ratio of 1:4 before day 8 of differentiation, and medium was replaced every 2–3 days.

Cell Proliferation Assays

Cell proliferation was assayed using CCK8 (Dojindo, Shanghai, China) and BrdU (MP Biomedicals) according to the manufacturer's instructions. For CCK8 detection, pNSCs from the TSC patient and normal control were plated in a 96-well plate at a density of 2×10^4 cells/100 μL/well, rapamycin (100 nM) was added 24 hr after cell plating, and cells were incubated for 24, 48, and 72 hr. Ten microliters of CCK8 was added to 100 μL of cultured cells. After 2 hr of incubation at 37°C in a humidified incubator containing 5% CO_2, the absorbance was detected at a wavelength of 450 nm.

For BrdU detection, after cell plating for 48 hr, BrdU was added to the culture medium for 4 hr, and the assay was performed according to the manufacturer's instructions.

Immunofluorescence

For immunofluorescence, TSC-patient-specific and unaffected control iPSCs, pNSCs, neurons, and astrocytes were fixed in 4% (w/v) paraformaldehyde at room temperature for 15 min, permeabilized for 15 min in PBS containing 0.5% (v/v) Triton X-100, blocked with 5% (w/v) BSA for 1 hr at room temperature, and incubated with primary antibodies overnight at 4°C in PBS containing 1% (w/v) BSA. Cells were then washed three times in PBS and incubated for 1 hr at room temperature with anti-rabbit or anti-mouse Alexa Fluor 488- and/or 555-conjugated secondary antibodies (Life Technologies). Cell nuclei were counterstained with 4′,6-diamidino-2-phenylindole. The primary antibodies used were as follows: rabbit anti-OCT4 (Abcam, catalog no. ab19857), rabbit anti-SOX2 (Abcam, catalog no. ab97959), mouse anti-SSEA4 (Abcam, catalog no. ab16287), mouse anti-TRA-1-81 (Abcam, catalog no. ab16289), mouse anti-AFP (Abcam, catalog no. ab3980), rabbit anti-SMA (Abcam, catalog no. ab5694), mouse anti-NESTIN (Life Technologies, catalog no. A24353), goat anti-SOX1 (Life Technologies, catalog no. A24354), rabbit anti-SOX2 (Life Technologies, catalog no. A24354), rabbit anti-PAX6 (Life Technologies, catalog no. A24354), rabbit anti-β-III-TUBULIN (TUJ1; Abcam, catalog no. ab18207), and rabbit anti-GFAP (Abcam, catalog no. ab7260).

Flow Cytometry Assay

Single cells derived from pNSCs were fixed and permeabilized following the manufacturer's instructions (BD Pharmingen). Cells were then stained with the following monoclonal fluorochrome-conjugated antibodies: PerCP-CY5.5 mouse anti-human SOX1, Alexa Fluor 647 mouse anti-NESTIN, and Alexa Fluor 488 mouse anti-human PAX6 (1 μg/mL per 1×10^6 cells [BD Biosciences, catalog nos. 560393, 561592, 561664]). Flow cytometry was performed using a FACSAria III flow cytometer (BD Biosciences), and data were analyzed using FACSDiva software (BD Biosciences). Fluorescence-activated cell sorting gating was based on the corresponding isotype control antibodies.

Immunoblotting

Western blotting of TSC-patient-specific and unaffected control pNSCs was performed as described previously. The primary antibodies used were rabbit anti-mTOR, anti-p-mTOR, anti-AKT, anti-pAKT, and anti-GAPDH (all from Cell Signaling, catalog nos. 2983S, 5536S, 4691S, 4060S, 2118S). Reactive proteins were visualized using an ImageQuant LAS 4000 mini system (GE Healthcare).

Neuron Morphology Quantification

Neuron morphology, including soma size, neurite length, and neurite branching complexity, was automatically quantified using ImageJ (NIH) with the NeurphologyJ plug-in (Ho et al., 2011).

Statistical Analysis

In all experiments, all available iPSC lines (three from the patient and three lines from two different control donors) were included. Data from continuous variables are expressed as mean ± SEM. Two-group comparisons were performed with the Student's t test. $p < 0.05$ was considered statistically significant. *$p < 0.05$, **$p < 0.01$, ***$p < 0.005$, ****$p < 0.001$.

SUPPLEMENTAL INFORMATION

Supplemental Information includes Supplemental Experimental Procedures and five figures and can be found with this article online at http://dx.doi.org/10.1016/j.stemcr.2017.02.020.

AUTHOR CONTRIBUTIONS

Y.L. performed the cell cultures, designed and performed the imaging experiments, analyzed the results, and wrote the manuscript; J.C. performed the immunohistochemistry experiments, analyzed the results, and wrote the manuscript; M.C. performed the western blot experiments, analyzed the results, and wrote the manuscript; Y.S. performed the flow cytometry assays and karyotype analysis; J.L. performed the TSC2 gene mutation analysis and RT-PCR. Y. Zhang performed the cell proliferation assays; Y. Zhu performed the teratoma formation experiments; L.W. performed neuronal differentiation and morphology quantification experiments; C.Z. supervised the research, coordinated the study, and wrote the manuscript.

ACKNOWLEDGMENTS

We thank Qian Yu for assistance with the induction of pluripotent stem cells and Dr. Bing Song for assistance with the flow cytometry assays. We thank Profs. Xiaofang Sun and Yong Fan of the Key Laboratory for Major Obstetric Disease of Guangdong Province, The Third Affiliated Hospital of Guangzhou Medical University for their valuable advice and comments on the manuscript. This work was supported by funding from the National Natural Science Foundation of China (nos. 81271401, 81471280).

Received: January 18, 2016
Revised: February 22, 2017
Accepted: February 23, 2017
Published: March 23, 2017

REFERENCES

Carson, R.P., Van Nielen, D.L., Winzenburger, P.A., and Ess, K.C. (2012). Neuronal and glia abnormalities in Tsc1-deficient forebrain and partial rescue by rapamycin. Neurobiol. Dis. *45*, 369–380.

Costa, V., Aigner, S., Vukcevic, M., Sauter, E., Behr, K., Ebeling, M., Dunkley, T., Friedlein, A., Zoffmann, S., Meyer, C.A., et al. (2016). mTORC1 inhibition corrects neurodevelopmental and synaptic alterations in a human stem cell model of tuberous sclerosis. Cell Rep. *15*, 86–95.

Crino, P.B. (2011). mTOR: a pathogenic signaling pathway in developmental brain malformations. Trends Mol. Med. *17*, 734–742.

Curto, G.G., Nieto-Estevez, V., Hurtado-Chong, A., Valero, J., Gomez, C., Alonso, J.R., Weruaga, E., and Vicario-Abejon, C. (2014). Pax6 is essential for the maintenance and multi-lineage differentiation of neural stem cells, and for neuronal incorporation into the adult olfactory bulb. Stem Cells Dev. *23*, 2813–2830.

Ebert, A.D., Yu, J., Rose, F.F., Jr., Mattis, V.B., Lorson, C.L., Thomson, J.A., and Svendsen, C.N. (2009). Induced pluripotent stem cells from a spinal muscular atrophy patient. Nature *457*, 277–280.

Endo, M., Antonyak, M.A., and Cerione, R.A. (2009). Cdc42-mTOR signaling pathway controls Hes5 and Pax6 expression in retinoic acid-dependent neural differentiation. J. Biol. Chem. *284*, 5107–5118.

Fathi, A., Hatami, M., Hajihosseini, V., Fattahi, F., Kiani, S., Baharvand, H., and Salekdeh, G.H. (2011). Comprehensive gene expression analysis of human embryonic stem cells during differentiation into neural cells. PLoS One *6*, e22856.

Han, J.M., and Sahin, M. (2011). TSC1/TSC2 signaling in the CNS. FEBS Lett. *585*, 973–980.

Henske, E.P., Scheithauer, B.W., Short, M.P., Wollmann, R., Nahmias, J., Hornigold, N., van Slegtenhorst, M., Welsh, C.T., and Kwiatkowski, D.J. (1996). Allelic loss is frequent in tuberous sclerosis kidney lesions but rare in brain lesions. Am. J. Hum. Genet. *59*, 400–406.

Ho, S.Y., Chao, C.Y., Huang, H.L., Chiu, T.W., Charoenkwan, P., and Hwang, E. (2011). NeurphologyJ: an automatic neuronal morphology quantification method and its application in pharmacological discovery. BMC Bioinformatics *12*, 230.

Jeganathan, D., Fox, M.F., Young, J.M., Yates, J.R., Osborne, J.P., and Povey, S. (2002). Nonsense-mediated RNA decay in the TSC1 gene suggests a useful tool pre- and post-positional cloning. Hum. Genet. *111*, 555–565.

Kandt, R.S., Haines, J.L., Smith, M., Northrup, H., Gardner, R.J., Short, M.P., Dumars, K., Roach, E.S., Steingold, S., Wall, S., et al. (1992). Linkage of an important gene locus for tuberous sclerosis to a chromosome 16 marker for polycystic kidney disease. Nat. Genet. *2*, 37–41.

Kwiatkowski, D.J., Palmer, M.R., Jozwiak, S., Bissler, J., Franz, D., Segal, S., Chen, D., and Sampson, J.R. (2015). Response to everolimus is seen in TSC-associated SEGAs and angiomyolipomas independent of mutation type and site in TSC1 and TSC2. Eur. J. Hum. Genet. *23*, 1665–1672.

Lasarge, C.L., and Danzer, S.C. (2014). Mechanisms regulating neuronal excitability and seizure development following mTOR pathway hyperactivation. Front. Mol. Neurosci. *7*, 18.

Long, X., Lin, Y., Ortiz-Vega, S., Yonezawa, K., and Avruch, J. (2005). Rheb binds and regulates the mTOR kinase. Curr. Biol. *15*, 702–713.

Magri, L., Cambiaghi, M., Cominelli, M., Alfaro-Cervello, C., Cursi, M., Pala, M., Bulfone, A., Garcia-Verdugo, J.M., Leocani, L., Minicucci, F., et al. (2011). Sustained activation of mTOR pathway in embryonic neural stem cells leads to development of tuberous sclerosis complex-associated lesions. Cell Stem Cell *9*, 447–462.

Mayer, K., Goedbloed, M., van Zijl, K., Nellist, M., and Rott, H.D. (2004). Characterisation of a novel TSC2 missense mutation in the GAP related domain associated with minimal clinical manifestations of tuberous sclerosis. J. Med. Genet. *41*, e64.

Onda, H. (2002). Tsc2 Null murine neuroepithelial cells are a model for human tuber giant cells, and show activation of an mTOR pathway. Mol. Cell Neurosci. *21*, 561–574.

Orlova, K.A., and Crino, P.B. (2010). The tuberous sclerosis complex. Ann. N. Y. Acad. Sci. *1184*, 87–105.

Seri, B., Garcia-Verdugo, J.M., McEwen, B.S., and Alvarez-Buylla, A. (2001). Astrocytes give rise to new neurons in the adult mammalian hippocampus. J. Neurosci. *21*, 7153–7160.

Talos, D.M., Kwiatkowski, D.J., Cordero, K., Black, P.M., and Jensen, F.E. (2008). Cell-specific alterations of glutamate receptor expression in tuberous sclerosis complex cortical tubers. Ann. Neurol. *63*, 454–465.

Tavazoie, S.F., Alvarez, V.A., Ridenour, D.A., Kwiatkowski, D.J., and Sabatini, B.L. (2005). Regulation of neuronal morphology and function by the tumor suppressors Tsc1 and Tsc2. Nat. Neurosci. *8*, 1727–1734.

Tyburczy, M.E., Wang, J.A., Li, S., Thangapazham, R., Chekaluk, Y., Moss, J., Kwiatkowski, D.J., and Darling, T.N. (2014). Sun exposure causes somatic second-hit mutations and angiofibroma development in tuberous sclerosis complex. Hum. Mol. Genet. *23*, 2023–2029.

Uhlmann, E.J., Apicelli, A.J., Baldwin, R.L., Burke, S.P., Bajenaru, M.L., Onda, H., Kwiatkowski, D., and Gutmann, D.H. (2002). Heterozygosity for the tuberous sclerosis complex (TSC) gene products results in increased astrocyte numbers and decreased p27-Kip1 expression in TSC2+/− cells. Oncogene *21*, 4050–4059.

van Slegtenhorst, M., de Hoogt, R., Hermans, C., Nellist, M., Janssen, B., Verhoef, S., Lindhout, D., van den Ouweland, A., Halley, D., Young, J., et al. (1997). Identification of the tuberous sclerosis gene TSC1 on chromosome 9q34. Science *277*, 805–808.

Yan, Y., Shin, S., Jha, B.S., Liu, Q., Sheng, J., Li, F., Zhan, M., Davis, J., Bharti, K., Zeng, X., et al. (2013). Efficient and rapid derivation of primitive neural stem cells and generation of brain subtype neurons from human pluripotent stem cells. Stem Cells Transl. Med. *2*, 862–870.